IMPACT OF A SATURATION-DEPENDENT DISSIPATION SOURCE TERM ON THE SKILL OF AN OPERATIONAL WIND-WAVE MODEL

Jose Henrique G. M. Alves[1], Diana J. M. Greenslade[2] and Michael L. Banner[1]

[1] School of Mathematics, University of New South Wales, 2052 Sydney, Australia
[2] Bureau of Meteorology Research Centre, Melbourne, AUstralia

1 INTRODUCTION

Compared to other coastal nations, Australia has one of the longest and most diverse coastlines, containing a wide range of climatic and oceanographic regions. These areas support nearly 90% of Australia's population. A significant part of this coastal population is directly or indirectly involved in activities related to the ocean, which include fishing, offshore petroleum and tourism. Commercial and industrial activities related to the marine environment generate more than AUD$30 billion per year. Sea-state forecasting plays an important role in providing strategic information for the success and safety of many of these activities.

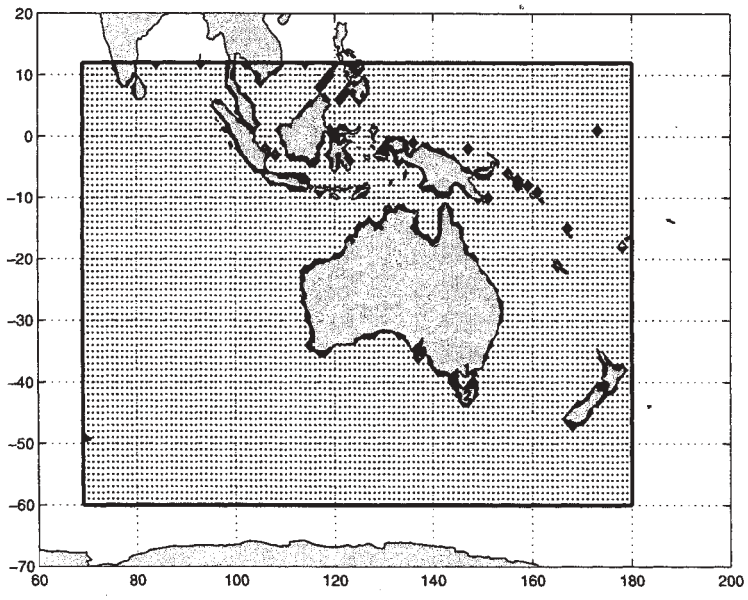

Figure 1: Regional implementation of the AUSWAM model. The numerical grid is shown as an array of black dots at the model resolution of 1 °. Ocean boundaries and coastlines of the numerical grid are indicated by thick continuous lines. Location of validation sites around the Australian coast are indicated by circles and labelled according to the definitions listed in Table 2.

Third-generation spectral wind-wave models are presently the basis of most operational sea-state forecasting systems worldwide. In the Australian Bureau of Meteorology (BoM), sea-state forecasts are generated by the AUSWAM model, a version of the WAM Cycle 4 model (Günther et al., 1992) with the following modifications: (i) a third-order numerical propagation scheme and (ii) source terms from the WAM Cycle 3 model. These two modifications of the standard WAM Cycle 4 release were based on numerical experiments reported in Bender and Leslie (1994) and Bender (1996), as discussed below.

In the absence of depth-induced effects and currents, the governing equation of spectral wave models reduces to the energy balance equation, as follows:

$$\left\{\frac{\partial}{\partial t}+\mathbf{c}_g\cdot\frac{\partial}{\partial \mathbf{x}}\right\}E(f,\theta)=S_{in}+S_{nl}+S_{ds}, \quad (1)$$

where $E(f,\theta)$ is the two-dimensional frequency spectrum, f is wave frequency, θ is wave direction, t is time, $\mathbf{c}_g$ is the wave group velocity, $\mathbf{x}$ is a position vector and the terms on the right-hand-side are source terms accounting for wind input (S_{in}), resonant nonlinear wave-wave interactions (S_{nl}) and dissipation (S_{ds}).

Extensive analytical and observational efforts have led to the development of acceptable parameterizations of S_{in}. In addition, third-generation wave models use robust forms of S_{nl} based on the theory of nonlinear interactions in a homogeneous wave field (Hasselmann, 1962; Zakharov, 1968). Due to the extreme difficulties involved in observing wave breaking and other dissipative processes in the field, dissipation is the least understood physical process driving wave development. Consequently, present models used in operational applications compute spectral dissipation rates through parametric functions developed mostly for tuning purposes.

Based on a conceptual framework for the onset of deep-water wave breaking due to the nonlinear modulation of wave groups, Alves and Banner (2000*b*) propose a new dissipation function that depends nonlinearly on the local azimuthally-integrated saturation spectrum $B = F(k)k^4$, where $F(k)$ is the azimuthally-integrated wavenumber spectrum. This new form of S_{ds} is successfully validated through numerical experiments of fetch-limited wind-wave evolution made with a research model featuring an exact solution for S_{nl} (Alves and Banner, 2000*b*) and an operational wind-wave model (Alves and Banner, 2000*a*).

The present study is a contribution towards testing the Alves-Banner dissipation source term [hereafter represented by the symbol S_{ds}^{ab}] using more realistic two-dimensional wind forcing conditions. For this purpose, S_{ds}^{ab} was implemented into AUSWAM. Performances of model hindcasts using several configurations of the new dissipation function were compared to the operational AUSWAM model setup. Model results were validated against *in situ* observations from two deep water sites off the Australian coast.

This manuscript is structured as follows. Section 2 provides a brief description of the implementation of AUSWAM presently used by the Australian Bureau of Meteorology. Buoy data and validation strategies are described in Section 3. Results are presented in Section 4, which is followed by concluding remarks and a list of references.

2 MODEL DESCRIPTION

The sea-state forecasting system at the Australian Bureau of Meteorology consists of three implementations of the AUSWAM model: (i) a global implementation at 3° spatial resolution; (ii) a regional model with 1° resolution, nested to the global model; and (iii) a mesoscale model running at 0.25° resolution, nested to the regional model. The regional AUSWAM implementation (Figure 1) covers an area from 60°S to 12°N and from 69°E to 180°E. The mesoscale model covers oceanic areas adjacent to the southeast of Australia. Regional and global operational implementations of AUSWAM also include a system to assimilate significant save height H_s observations from the European Remote-Sensing Satellite ERS-2 (Greenslade, 1999).

The AUSWAM model is a modified version of the WAM model. WAM is a third-generation spectral wind-wave model that describes the evolution of the two-dimensional frequency spectrum $E(f,\theta)$ with respect to frequency f and direction θ. Spectral evolution is calculated by integrating the action balance equation in its spherical coordinate form

$$\frac{\partial E}{\partial t}+\cos^{-1}\phi\frac{c_\phi\cos\phi E}{\partial\phi}+\frac{\partial c_\lambda E}{\partial\lambda}+\frac{\partial c_\theta E}{\partial\theta}=S_{in}+S_{nl}+S_{ds}, \quad (2)$$

where $c_{\phi,\lambda,\theta}$ are components of the group velocity

AUTHOR INDEX TABLE OF CONTENTS

$\mathbf{c}_g = g/4\pi f$ in latitude ϕ, longitude λ and direction θ and S_{in}, S_{nl} and S_{ds} are the wind input, nonlinear interactions and dissipation source functions, respectively. AUSWAM uses the Direct Interaction Approximation (DIA) of S_{nl}, following Hasselmann and Hasselmann (1985), and parameterised S_{in} and S_{ds} source terms consistent with the physics used in the WAM Cycle 3 release.

The wind input source term follows the general form proposed by Snyder et al. (1981):

$$S_{in}(f,\theta) = C_{in} \quad \frac{\rho_{air}}{\rho_{water}} \omega \left(\frac{U_0}{C}\cos\theta - 1\right) E(f,\theta), \tag{3}$$

where $C_{in} = 0.25$ is a constant of proportionality, ρ specifies the density of air or water and U_0 is a scaling wind speed.

The WAM model uses a S_{in} defined in terms of the friction velocity through the relation $U_0 = 28u_*$ (Komen et al., 1984). In the original Snyder et al. (1981) form, the 5m-height wind is used ($U_0 = U_5$). In this study, model validation tests were made with two forms of S_{in} specified in terms of both U_5 and $28u_*$. In the standard AUSWAM operational implementation, whitecap dissipation is computed according to the quasilinear source term proposed by Komen et al. (1984), as follows:

$$S_{ds}^{w3}(f,\theta) = -C_{ds} \quad \left(\frac{\hat{\alpha}}{\hat{\alpha}_{PM}}\right)^m \left(\frac{\omega}{\overline{\omega}}\right)^n \bar{\omega} E(f,\theta), \tag{4}$$

where $\hat{\alpha} = E_{tot}\overline{k}^2$ is an integral steepness parameter and $\overline{k}$ and $\overline{\omega}$ are the mean wavenumber and radian frequency, respectively. In AUSWAM, the value of the dissipation coefficient $C_{ds} = 6.74 \times 10^{-5}$ was set according to Bender and Leslie (1994), while Komen et al. (1984) suggest a somewhat lower constant $C_{ds} = 3.33 \times 10^{-5}$. Other S_{ds} parameters used in AUSWAM were unmodified relative to the standard WAM Cycle 3 release (i.e., $m = 2$ and $n = 2$).

	S_{ds}				
Run code	C_{ds}	m	n	p_∞	B_r
BOM	6.74×10^{-5}	2.0	2.0		
WM3	3.33×10^{-5}	2.65	2.0		
AB1	7.71×10^{-2}	1.3	1.0	0.0	
AB2	2.63	2.0	0.0	4.0	7.5×10^{-3}
AB3	1.91	2.0	0.0	4.0	5.8×10^{-3}
AB4	8.80×10^{-3}	1.0	1.0	4.0	5.0×10^{-3}

Table 1: Summary of run codes and dissipation parameters.

The new dissipation function S_{ds}^{ab} proposed by Alves and Banner (2000*b*) is based on the assumption that spectral dissipation rates of dominant waves are primarily determined by breaking due to the modulation of nonlinear wave groups. This effect is computed through a term that depends nonlinearly on a local measure of wave steepness, represented by the saturation spectrum $B(k,\theta) = F(k,\theta)k^4$. A general expression for S_{ds}^{ab} is given by

$$S_{ds}^{ab}(f,\theta) = -C_{ds} \quad \left(E_{tot}k_p^2\right)^m \left(\frac{k}{\overline{k}}\right)^n \left(\frac{B(k)}{B_r}\right)^{p/2} \omega E(f,\theta), \tag{5}$$

where C_{ds} is a constant setting overall dissipation levels, E_{tot} is the total energy, k_p and $\overline{k}$ are the peak and mean wavenumbers, $B(k) = k^4F(k)$ is the azimuthally integrated spectral saturation parameter, B_r is a reference saturation level, m and n are constant exponents and p, the exponent of the term representing dissipation due to nonlinear group modulation, is given by

$$p = \frac{p_\infty}{2} + \tag{6}$$

$$\frac{p_\infty}{2} \quad \tanh\left\{10\left(\sqrt{\frac{B(k)}{B_r}}-1\right)\right\}.$$

Equation (6) prescribes p as a function that fluctuates between zero and p_∞ whenever the local integrated saturation level $B(k)$ is below or above the threshold saturation value B_r, respectively. The spectral dissipation rates will, therefore, be dominated by the term dependent on the local saturation level whenever $B(k) > B_r$. For values of $B(k) < B_r$, $p \to 0$ and the term $(B(k)/B_r)^{p/2}$ asymptotes to unity. Dissipation rates will then be determined by the remaining terms $(E_{tot}k_p^2)^m$ and $(k/\overline{k})^n$, describing background energy losses.

3 VALIDATION STRATEGY

This study presents a comparison of hindcasts generated by the AUSWAM model using six alternative configurations of S_{ds}, corresponding to the standard AUSWAM dissipation term, an optimised variation of the WAM Cycle 3 term and four variations of the Alves-Banner saturation-dependent form S_{ds}^{ab}. Experiments were labeled with the prefixes BOM, WM3 and AB, respectively. Dissipation parameters used in the six alternative hindcast experiments are summarised in Table 1.

Parameters of S_{ds}^{ab} listed in Table 1 were determined through fetch-limited experiments made with AUSWAM, as described in Alves and Banner (2000*a*). In these experiments, S_{ds}^{ab} was manually tuned to produce model results matching the empirical fetch-limited evolution curves of Kahma and Calkoen (1992) and the fully-developed limits proposed by Alves et al. (2000).

Table 1 shows that the configuration of S_{ds}^{w3} used in the AUSWAM model (run BOM) adopts a constant $C_{ds} = 6.74 \times 10^{-5}$ that is significantly higher than the original constant value $C_{ds} = 3.33 \times 10^{-5}$ from WAM Cycle 3 release (run WM3). This change in C_{ds} was justified on the basis of a wave hindcast study performed by Bender and Leslie (1994) over a one-month period that did not include a validation of the atmospheric model winds used to force the wave model. The specification of this higher dissipation rate level may have resulted from the need to compensate for overpredictions in wind fields generated by the LAPS model.

The configuration of S_{ds}^{w3} used in run WM3 is a slight variation of the original WAM Cycle 3 setup in which the exponent m is increased from 2 to 2.65. This value of m was determined by Monbaliu and Hasselmann (1994) through an automatic model optimisation method. Other dissipation parameters correspond to the original WAM Cycle 3 configuration of S_{ds}^{w3} (i.e., $m = 2$ and $n = 2$).

Label	Code	Location	Hull type	Payload	Position Lat	Position Long	Depth (m)	Wind height	Sample rate (h)
1	55039	Bass Strait	EMI Sensor	Esso	-38.60	148.19	75	44.0	1/6
2	55026	Strahan	Waverider	BoM	-42.08	145.01	100	19.5	1/2

Table 2: Characteristics and locations of wind and wave measurement sites used for model validation. Numbers in the first column correspond to labels in Figure 1. Codes are the World Meteorological Organization (WMO) index numbers.

Wave hindcasts analysed in the present study were generated using wind fields from a 62 day period between March 20 00Z and May 20 00Z 1998. Winds were obtained from analysed data produced by the regional atmospheric model LAPS (Puri et al., 1998) used at the BoM. The performances of the alternative S_{ds} configurations of Table 1 were compared and ranked according to the values of four statistical parameters [bias, root mean square (rms) error, scatter index and correlation coefficient] calculated in relation to H_s and T_p data at the two validation sites (Bass Strait and Strahan) shown in Figure 1. The statistical parameters are defined as follows:

(i) Bias

$$bias = \frac{\sum_{i=1}^{N} M_i - O_i}{N}; \qquad (7)$$

(ii) Root-mean-square error

$$\epsilon_{rms} = \sqrt{\frac{\sum_{i=1}^{N}(M_i - O_i)^2}{N}}; \qquad (8)$$

(iii) Scatter index

$$SI = \frac{\sigma_M}{\overline{O}}; \qquad (9)$$

(iv) Correlation coefficient

$$r = \frac{\sum_{i=1}^{N}(O_i - \overline{O})(M_i - \overline{M})/N}{\sqrt{\sum_{i=1}^{N}(O_i - \overline{O})^2}\sqrt{\sum_{i=1}^{N}(M_i - \overline{M})^2}} \qquad (10)$$

where O_i and M_i represent observed and modelled values, respectively, of either wind speed U_{10}, wind direction θ_U, significant wave height H_s or spectral peak wave period T_p; σ_M is the standard deviation of modelled values; N is the number of observations; and over-bars denote ensemble averages. All statistics were determined by assuming that observations provided the best estimate of the true value of each diagnostic variable.

Model hindcasts were validated against H_s and T_p data from the two sites shown in Figure 1. Table 2 provides a list of their relevant characteristics. Measurements in Bass Strait were made with an electromagnetic induction sensor attached to the leg of an oil platform. In Strahan, measurements were made with a Datawell Waverider buoy. Observations were assumed to be made in deep water. Data from Bass Strait and Strahan, sampled at 10 and 30 min respectively, were reduced to one-hourly intervals by simple averaging. Following the approach of Cardone et al. (1994), the resulting hourly time series were smoothed by averaging three successive observations with weights 1/4, 1/2 and 1/4, to reduce sampling variability. Smoothed hourly time series were finally sub-sampled at three-hourly intervals at times corresponding to the wave model outputs.

Measurements of wind velocity and direction were made at different anemometer heights, as indicated in Table 2. To allow the validation of the hindcast 10m-height wind fields used to force AUSWAM, available observations were converted into corresponding 10m-height winds by assuming a neutrally-stable logarithmic atmospheric boundary layer. Converted U_{10} values were derived using the relation

$$U_z = U_{10}\ln(z/z_0)/\ln(10/z_0), \qquad (11)$$

where the roughness length z_0 was determined from the Charnock relation and the drag coefficient parameterisation proposed by Wu (1982). Although in non-neutral atmospheric stability conditions the wind profile may deviate from this logarithmic profile, measurements of the air-sea temperature differences were not available. As a proper estimation of stability conditions could not be made, neutral stability was assumed.

In most cases, nodes from the regional model grid did not match exactly the location of measurement sites. Because of the relatively coarse resolution of this numerical grid (i.e., 1°) and the proximity of measurement sites to the coast, it was not possible to spatially interpolate the model output into the exact buoy locations, as this would involve nodes over land boundaries. Consequently, model validation was performed using the output from grid nodes nearest to each buoy location.

Both global and regional implementations of AUSWAM were run with the available 62-day LAPS wind-fields. Data assimilation was switched off so that the contrast between different wave model physics options could be emphasised. Initialisation occurred at day 1 the hindcast period with analysed spectra obtained from the BoM operational archives. The global model was run only once with the standard BoM model physics, corresponding to S_{in} and S_{ds} prescribed by equations (3) and (4), respectively. Wave model spectra from the global model at the borders of the regional model were stored and used as boundary conditions for the nested regional model runs. Boundary conditions were, therefore, identical in all regional simulations.

Site	U_{10}					θ_U			
	U_{10}^{obs} m/s	*bias* m/s	ϵ_{rms} m/s	*SI*	r	*bias* deg	ϵ_{rms} deg	*SI*	r
Bass Strait	6.53	0.48	2.15	0.32	0.86	127	74.80	0.38	0.69
Strahan	6.41	1.45	2.79	0.37	0.81	30.99	97.07	0.44	0.54

Table 3: Validation of wind speed U_{10} and direction θ_U at Bass Strait and Strahan during the hindcast period of March 20 to May 20 1998. Listed statistical parameters are bias, root mean square error ϵ_{rms}, scatter index SI and correlation coefficient r. Mean observed values of wind speed U_{10}^{obs} are also indicated.

The propagation time step was set to 20 minutes. Source terms were integrated every 10 minutes. The discrete representation of the two-dimensional frequency spectrum $E(f,\theta)$ consisted of 25 frequency bins logarithmically spaced from 0.0418 Hz to 0.4114 Hz, at intervals of $\Delta f/f = 0.1$, and 12 directional bins with 30° resolution. These general setting were used in both global and regional model runs.

At 1° and 3° spatial grid resolution, very few of the wave model grid points were in water depths of less than 100m. Therefore, the regional and global wave models were run with deep water physics only (i.e., bottom friction and refraction effects were switched off). Modelled wave spectra and diagnostic variables such as significant wave height H_s, mean wave direction θ_m and peak period T_p were stored in output files at 3 model-hour intervals.

The global wave model was forced with 12-hourly hindcast winds at 2.5° spatial resolution, obtained from the global atmospheric model GASP (Seaman et al., 1995) at the BoM. Winds used to force the regional wave model were obtained from the regional atmospheric model LAPS (Puri et al., 1998). Proper U_{10} values were converted from the nearest atmospheric model level via Monin-Obukhov theory with empirical stability functions given by Garrat (1992), in both cases. Furthermore, wind fields were interpolated into hourly intervals and reduced to the required spatial resolution of each model grid. Experiments were performed in a 32 vector processor NEC SX-4 supercomputer, which is largely dedicated to running operational models that produce weather and sea-state forecasts for the Australian region on a 12-hourly basis.

4 RESULTS

Validation statistics of Wind speeds generated by the LAPS model in Bass Strait and Strahan are shown in Table 3. Although the validation statistics shown in Table 3 indicate that the bulk of LAPS model wind fields is not ideal for a critical overall evaluation of wave model performance, model winds in Bass Strait and Strahan were in relatively good agreement with observations. A refined analysis comparing the performance of the saturation-dependent dissipation term S_{ds}^{ab} with the standard AUSWAM configuration using higher quality winds will be provided in a forthcoming paper.

Scatterplots of hindcast and observed H_s and T_p in Bass Strait during the 62-day period of March 20 to May 20 1998 are shown in Figures 2 and 3, respectively. A linear least squares fit through the cloud of co-located data suggests that most alternative experiments generated good hindcast significant wave heights. An exception was run WM3, which produced hindcasts with a strong bias towards overestimating most measurements of H_s. On the other hand, hindcast T_p from all model runs had a consistent trend towards underestimation of measurements greater than approximately 8s.

Table 4 lists the validation statistics corresponding to the Bass Strait hindcasts shown in Figures 2 and 3. Statistics of hindcast H_s indicate a best overall performance of runs BOM, AB1 and AB2. Hindcasts from runs AB3 and AB4 also produced good statistical scores. Run WM3, however, generated hindcast H_s with high positive bias, rms error and scatter index. Although values of bias, rms error and scatter index were comparable to those of hindcast H_s, the correlation coefficients of hindcast T_p were remarkably low (under 0.35 in all cases).

This lower correlation of hindcast T_p values in Bass Strait, which was particularly strong at larger values of this parameter (e.g., $T_p > 8$s), suggests that the ratio between the energy of swell and wind-seas is incorrect in the wave model results. This discrepancy may be associated with at least three factors: (i) the poor specification of swell properties at the external boundary of the regional model grid, (ii) the excessive dissipation of low frequency spectral components in the different specifications of S_{ds} and (iii) the coarse resolution of the regional model grid within Bass Strait. As discussed previously, the first two factors cannot be directly assessed due to the lack of observed wave spectra near the outer regional grid boundaries.

Figure 1 shows that the complex land features within Bass Strait were considerably simplified due to the coarse resolution (1°) of the regional model grid. This misrepresentation does not affect local operational sea-state forecasts, as these are based on the results of a higher resolution (0.25°) meso-scale implementation of AUSWAM covering the southeastern region of the Australian continent in more detail. This implementation, however, was not available for the experiments described in this study.

A visual examination of the available time series of regional hindcasts and observations of T_p generated with alternative forms of S_{ds} revealed that model data within Bass Strait systematically omitted wave events with peak periods typically greater than 12s, usually associated with the occurrence of weak local winds. This combination of higher T_p values with weak local winds is a well-recognised characteristic of swell events. Due to the frequent development of mid-latitude cyclones within the Southern Ocean, these swell systems may often penetrate Bass Strait through its western entrance. This passage, however, is almost completely blocked in the regional model grid, as seen in Figure 1. This numerical boundary may have, consequently, obstructed the passage of swell in the regional simulations, leading to the disagreement between model hindcasts and observations of T_p seen in Table 4 and in Figure 3.

March/May 1998			H_s				T_p			
Location	Mean obs	Run	*bias* m/s	ϵ_{rms} m/s	*SI*	*r*	*bias* sec	ϵ_{rms} sec	*SI*	*r*
Bass Strait	$\overline{H_s^{obs}} = 1.57$m	BOM	-0.16	0.49	0.29	0.86	-1.39	2.81	0.28	0.32
	$\overline{T_p^{obs}} = 8.79$s	WM3	0.37	0.65	0.34	0.85	-0.23	2.40	0.27	0.31
		AB1	-0.12	0.43	0.27	0.87	-1.28	2.58	0.26	0.33
		AB2	0.09	0.42	0.26	0.86	-1.68	2.70	0.24	0.26
		AB3	0.30	0.52	0.27	0.86	-0.97	2.38	0.25	0.25
		AB4	-0.23	0.51	0.29	0.86	-2.67	3.57	0.27	0.13
Strahan	$\overline{H_s^{obs}} = 3.44$m	BOM	-0.73	1.12	0.25	0.77	-2.62	3.67	0.20	0.36
	$\overline{T_p^{obs}} = 12.99$s	WM3	0.53	1.06	0.27	0.80	-0.58	2.30	0.17	0.41
		AB1	-0.41	0.85	0.22	0.79	-1.74	2.75	0.16	0.38
		AB2	-0.38	0.89	0.23	0.77	-3.43	4.06	0.17	0.31
		AB3	0.10	0.79	0.23	0.81	-2.50	3.33	0.17	0.33
		AB4	-1.10	1.40	0.25	0.74	-4.56	5.11	0.18	0.26

Table 4: Validation statistics from hindcasts of significant wave height H_s and peak period T_p provided by AUSWAM at sites 55039 (Bass Strait) and 55026 (Strahan) during the period of March 20 to May 20 1998. Listed statistical parameters are bias, root mean square error ϵ_{rms}, scatter index *SI* and correlation coefficient *r*.

Figures 4 and 5 show the comparisons of hindcast and observed H_s and T_p in Strahan. The difference of results from model runs using alternative S_{ds} configurations is greater than in the data from Bass Strait. Lines of least squares fit through the co-located data suggest that hindcasts of H_s from runs BOM, AB1, AB2 and AB4 systematically underestimated the observations. On the other hand, hindcast H_s produced by run WM3 overestimated the observed values. Only hindcast H_s from run AB3 were in good agreement with the observations, as indicated by their low bias. The general trends seen in the scatterplots of hindcast and observed T_p from Strahan, however, repeat those seen in data from Bass Strait: most model runs underestimated higher values of peak period. An exception were the

results from run WM3, which were in better agreement with observations.

Validation statistics shown in Table 4 indicate that the hindcasts of H_s from run AB3 had the lowest bias and rms error, and thus the best overall performance in both measurement sites. The low scatter index of this model run is, nevertheless, comparable to that of runs AB1 and AB2. These two cases also delivered a good performance in terms of bias and rms error. Runs BOM and AB4 produced significant negative bias and high rms errors. Their scatter-indices, however, were slightly improved relative to run WM3. This latter experiment generated hindcast H_s with considerable positive bias and high rms error.

Run WM3 provided the lowest values of bias in terms of hindcast T_p in both Strahan and Bass Strait. The lowest rms errors in these two locations were associated with runs WM3, AB1 and AB3, while scatter indices of these three test cases and those of runs AB2 were all remarkably low. The poor performance of run AB4 in Strahan and Bass Strait indicates that its configuration of S_{ds}^{ab} may be predicting too much dissipation at wavenumbers lower than the peak. Despite these apparent differences, all model runs correlated poorly with the trends of measured T_p, as suggested by the low values of the parameter r. This generally poor agreement with observations supports the idea that either swell systems are not being properly specified at the AUSWAM model boundaries or, alternatively, that most forms of S_{ds} used in this study predicted dissipation rates that were too high for low wavenumbers. These issues are currently being investigated.

5 CONCLUDING REMARKS

The present study investigates the impact of a new formulation for the dissipation source term S_{ds} on the skill of AUSWAM, the wind-wave model used by the Australian Bureau of Meteorology to produce official sea-state forecasts. The new form of S_{ds} features a nonlinear dependence of spectral dissipation rates on the azimuthally integrated saturation parameter $B(k) = k^4 F(k)$. Model hindcasts of significant wave height H_s and peak period T_p are validated at two measurement sites off the Australian coast. Hindcasts are generated with (i) the standard AUSWAM dissipation term, (ii) an optimised variation of the WAM Cycle 3 term and (iii) four variations of the newly-proposed saturation-dependent form of S_{ds}.

The validation of alternative AUSWAM model hindcasts of H_s and T_p in two validation sites (Strahan and Bass Strait) may be summarised as follows:

- the configuration of S_{ds} used in the standard AUSWAM model setup (run BOM), consisting of the WAM Cycle 3 dissipation function S_{ds}^{w3} with an increased value of the constant C_{ds}, produced hindcasts of H_s and T_p that generally underestimated measured data;

- the alternative configuration of S_{ds}^{w3} used in run WM3 provided the best hindcasts of T_p. This good relative performance is probably related to its stronger nonlinear dependence on the integrated steepness parameter $(E_{tot}\overline{k}^2)^m$. In association with a lower value of C_{ds} relative to the standard AUSWAM configuration, this may have reduced significantly the dissipation levels of old wind seas, leading to a more unconstrained growth of swell components of the wave spectrum. This benefit, however, had as a tradeoff the systematic overestimation of hindcast H_s at both validation sites;

- the aim of run AB1 was to examine the effect of redefining the integral steepness parameter of S_{ds}^{w3} as a function of the peak wavenumber k_p (i.e., the form $E_{tot}\overline{k}^2$ used in S_{ds}^{w3} was replaced by $E_{tot}k_p^2$), as discussed in Alves and Banner (2000*a*). This change may explain why this experiment provided improved hindcast H_s when compared to results of runs BOM and WM3. Hindcasts of T_p from run AB1 were also consistent with observations;

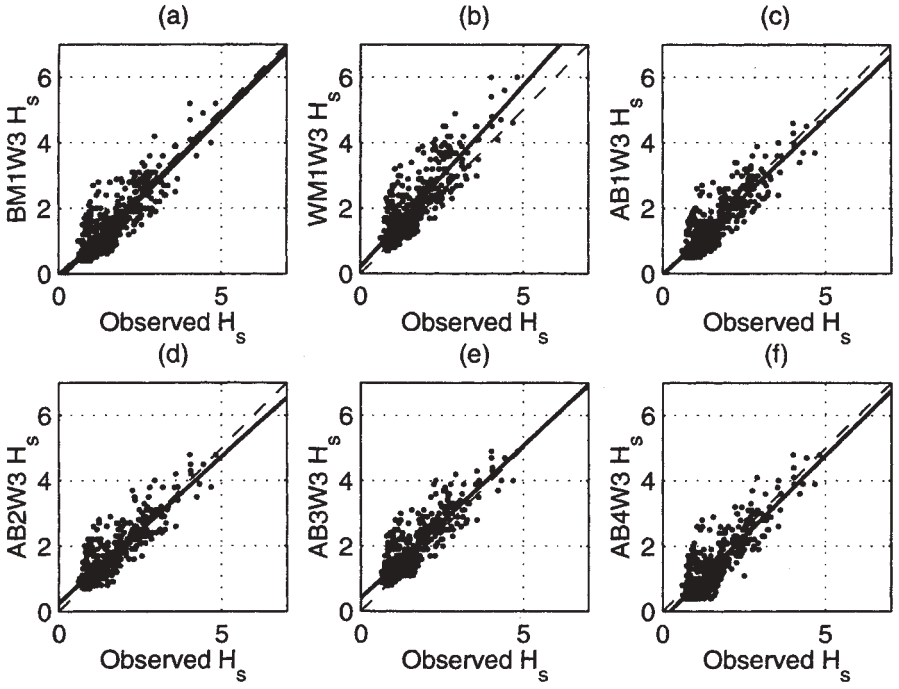

Figure 2: Scatterplots of hindcast and observed significant wave heights H_s in Bass Strait during March 20 to May 20 1998. Model runs are indicated in the vertical axis. Thin dashed lines indicate a perfect 1-to-1 correlation and continuous lines indicate the linear least squares fit through the cloud of co-located data.

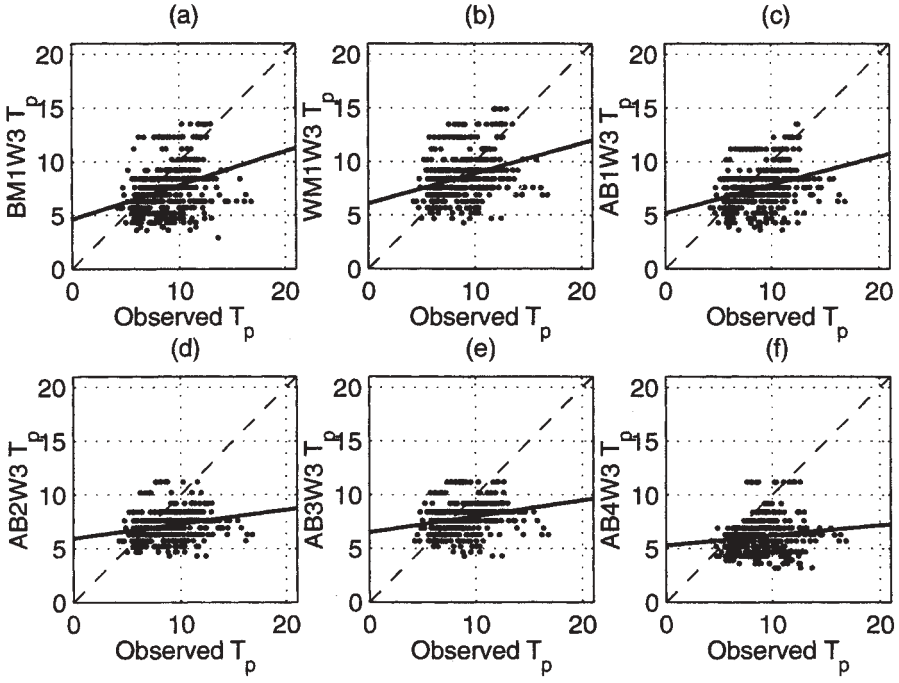

Figure 3: Scatterplots of hindcast and observed significant peak periods T_p in Bass Strait during March 20 to May 20 1998. Model runs are indicated in the vertical axis. Thin dashed lines indicate a perfect 1-to-1 correlation and continuous lines indicate the linear least squares fit through the cloud of co-located data.

- statistics of hindcast H_s from runs AB2 and AB3, made with a strong dependence of S_{ds} on the saturation parameter $B(k)$, were in excellent agreement with measurements. In sta-

tistical terms they were generally superior to cases using the WAM Cycle 3 form of S_{ds} (BOM and WM3). Statistics of hindcast T_p from runs AB2 and AB3, however, indicated that the dissipation rates of spectral components within the swell range predicted by S_{ds}^{ab} may need to be reduced;

- run AB4 produced the most degraded hindcasts of H_s and T_p. This may be a consequence of its stronger dependence on the weighting term $(k/\overline{k})^n = 1$, which increases the dissipation rates at wavenumbers higher than the peak and of incorrect tuning of other dissipation parameters.

These conclusions indicate that the newly-proposed saturation-dependent form S_{ds}^{ab} generally improves the hindcasts of sea-state produced by the AUSWAM model in terms of H_s. Discrepancies in the hindcasts of peak periods, however, indicate that further adjustments are needed in the specification of dissipation rates at wavenumbers lower than the spectral peak. Nevertheless, validation statistics of hindcast T_p from test cases using S_{ds}^{ab} were in the majority of cases better than those associated with the standard AUSWAM setup. These positive results demonstrate the potential benefits of using this new saturation-dependent form of S_{ds} in operational wind-wave models.

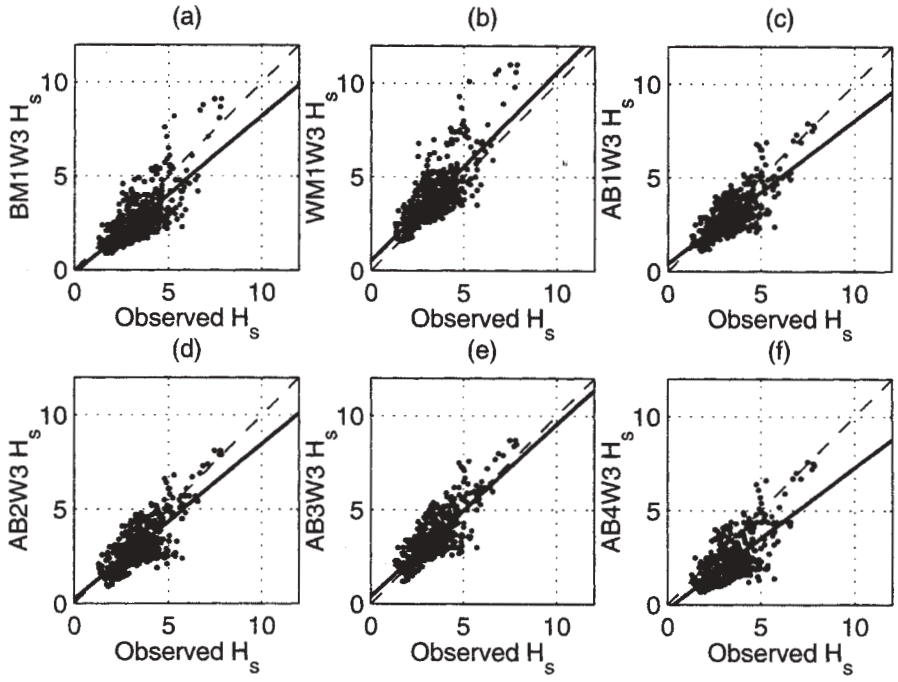

Figure 4: Scatterplots of hindcast and observed significant wave heights H_s in Strahan during the second hindcast period of March 20 to May 20 1998. Model runs are indicated in the vertical axis. Thin dashed lines indicate a perfect 1-to-1 correlation and continuous lines indicate the linear least squares fit through the cloud of co-located data.

6 ACKNOWLEDGEMENTS

The authors acknowledge the Australian Bureau of Meteorology Research Centre (BMRC) for providing the numerical model and the computational resources used in this investigation. This study was part of the doctoral thesis research activities of the first author (J.H.G.M.A.), made possible through a scholarship provided by the Conselho Nacional de Desenvolvimento Cientifico e Tecnologico (CNPq) of Brazil.

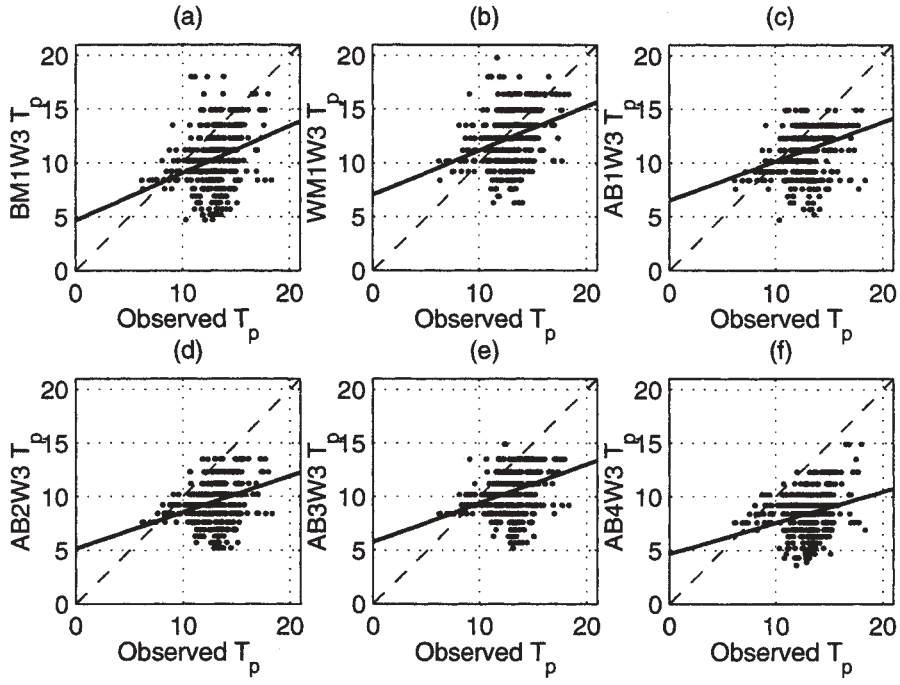

Figure 5: Scatterplots of hindcast and observed significant wave heights (upper panels) and peak periods T_p (lower panels) in Strahan during March 20 to May 20 1998. Model runs are indicated in the vertical axis. Thin dashed lines indicate a perfect 1-to-1 correlation and continuous lines indicate the linear least squares fit through the cloud of co-located data.

REFERENCES

Alves, J. H. G. M. and M. L. Banner (2000*a*), Impact of a saturation-dependent dissipation funciton on wind-wave models: fetch-limited case, *in* '27th International Conference on Coastal Engineering (Abstracts)', Vol. 1, ASCE, Sydney.

Alves, J. H. G. M. and M. L. Banner (2000*b*), 'A saturation-dependent dissipation function for wind-wave modelling applications. Part I: Fetch-limited experiments'. In preparation.

Alves, J. H .G. M., M. L. Banner and I. R. Young (2000), 'Revisiting the asymptotic limits of fully-developed seas', *J. Phys. Oceanogr.* . Submitted.

Bender, L. C. (1996), 'Modification of the physics and numerics in a third-generation ocean wave model', *J. of Atmos. Oceanic Tech.* **13**(3), 726–750.

Bender, L. C. and L. M. Leslie (1994), Evaluation of a third-generation ocean wave model for the australian region, BMRC Research Report 43, Bureau of Meteorology Research Centre, Melbourne, Australia.

Cardone, V. J., H. C. Graber, R. E. Jensen, S. Hasselmann and M. J. Caruso (1994), 'In search of the true surface wind field in SWADE IOP-1: ocean wave modelling perspective', *Global Atm. Ocean Syst.* **3**, 107–150.

Garrat, J. R. (1992), *The atmospheric boundary layer*, University Press, Cambridge. 316pp.

Greenslade, D. (1999), The assimilation of ERS-2 significant wave height data in the Australian wave model, BMRC Research Report 73, Bureau of Meteorology, Melbourne, Australia.

Günther, H., S. Hasselmann and P. A. E. M. Janssen (1992), The WAM model Cycle 4, Technical Report 4, German Climate Research Center - DKRZ, Hamburg.

Hasselmann, K. (1962), 'On the nonlinear energy transfer in a gravity-wave spectrum. Part 1: General theory', *J. Fluid Mech.* **12**, 481–500.

Hasselmann, S. and K. Hasselmann (1985), 'Computations and parameterizations of the nonlinear energy transfer in a gravity-wave spectrum. Part 1: a new method for efficient computations of the nonlinear transfer integral', *J. Phys. Oceanogr.* **15**, 1369–1377.

Kahma, K. and C. J. Calkoen (1992), 'Reconciling discrepancies in the observed growth of wind-generated waves', *J. Phys. Oceanogr.* **22**, 1389–1405.

Komen, G. J., S. Hasselmann and K. Hasselmann (1984), 'On the existence of a fully developed wind-sea spectrum', *J. Phys. Oceanogr.* **14**(8), 1271–1285.

Monbaliu, J. and S. Hasselmann (1994), Optimization of the WAM source functions by direct cost function minimization, *in* G. J. K.et al., ed., 'Dynamics and modelling of wind waves', Cambridge University Press, Cambridge, pp. 442–447.

Puri, K., G. S. Dietachmayer, G. A. Mills, N. E. Davison, R. A. Bowen and L. W. Logan (1998), 'The new BMRC limited area prediction system', *Aust. Met. Mag.* **47**, 203–233.

Seaman, R, W. Bourke, P. Steinle, T Hart, G. Embery, M. Naughton and L. Rikus (1995), 'Evolution of the Bureau of Meteorology's global assimilation and prediction system. Part 1: analyses and initialization', *Aust. Met. Mag.* **44**, 1–18.

Snyder, R. L., F. W. Dobson, J. A Elliot and R. B. Long (1981), 'Array measurements of atmospheric pressure fluctuations above surface gravity waves', *J. Fluid Mech.* **102**, 1–59.

Wu, J. (1982), 'Wind-stress coefficients over the sea surface from breeze to hurricane', *J. Geophys. Res.* **87 (C12)**, 9704–9706.

Zakharov, V. E. (1968), 'Stability of periodic waves of finite amplitude on the surface of a deep fluid', *J. Appl. Mech. Techn. Phys.* **9**, 190–194.